Solution Structure of Rat Apo-S100B($\beta\beta$) As Determined by NMR Spectroscopy[†,‡]

Alexander C. Drohat,[§] Judith C. Amburgey,[§,||] Frits Abildgaard,[⊥] Mary R. Starich,[#,□] Donna Baldisseri,[§] and David J. Weber*[,§]

Department of Biochemistry and Molecular Biology, University of Maryland School of Medicine, Baltimore, Maryland 21201, The Howard Hughes Medical Institute and Department of Chemistry and Biochemistry, University of Maryland Baltimore County, Baltimore, Maryland 21228, and The National Magnetic Resonance Facility at Madison, University of Wisconsin at Madison, Madison, Wisconsin 53706-1569

Received May 22, 1996; Revised Manuscript Received July 3, 1996[⊗]

ABSTRACT: S100B($\beta\beta$), a member of the S100 protein family, is a Ca^{2+}-binding protein with noncovalent interactions at its dimer interface. Each apo-S100β subunit (91 residues) has four α-helices and a small antiparallel β-sheet, consistent with two predicted helix−loop−helix Ca^{2+}-binding domains known as EF-hands [Amburgey *et al.* (1995) *J. Biomol. NMR 6,* 171−179]. The three-dimensional solution structure of apo-S100B($\beta\beta$) from rat has been determined using 2672 distance (14.7 per residue) and 88 dihedral angle restraints derived from multidimensional nuclear magnetic resonance spectroscopy. Apo-S100B($\beta\beta$) is found to be globular and compact with an extensive hydrophobic core and a highly charged surface, consistent with its high solubility. At the symmetric dimer interface, 172 intermolecular nuclear Overhauser effect correlations (NOEs) define the antiparallel alignment of helix I with I′ and of helix IV with IV′. The perpendicular association of these pairs of antiparallel helices forms an X-type four-helical bundle at the dimer interface. Whereas, the four helices within each apo-S100β subunit adopt a unicornate-type four-helix bundle, with helix I protruding from the parallel bundle of helices II, III, and IV. Accordingly, the orientation of helix III relative to helices I, II, and IV in each subunit differs significantly from that known for other Ca^{2+}-binding proteins. Indeed, the interhelical angle (Ω) observed in the C-terminal EF-hand of apo-S100β is −142°, whereas Ω ranges from 118° to 145° in the apo state and from 84° to 128° in the Ca^{2+}-bound state for the EF-hands of calbindin D_{9k}, calcyclin, and calmodulin. Thus, a significant conformational change in the C-terminal EF-hand would be required for it to adopt a structure typical of the Ca^{2+}-bound state, which could readily explain the dramatic spectral effects observed upon the addition of Ca^{2+} to apo-S100B($\beta\beta$).

S100B, a dimeric Ca^{2+}-binding protein, is a member of the highly conserved S100 protein family. S100B was originally discovered at high concentration in glial cells; however, it is now known to be expressed in a wide variety of tissues and cell lines including malignant tumors (Moore, 1965; Kligman & Hilt, 1988; Donato, 1991; Zimmer *et al.*, 1995). The gene for the S100B subunit (S100β) is mapped to the Down's syndrome region of human chromosome 21 (bands 21q22.2 and 22.3), and levels of S100β[1] are significantly increased in activated astrocytes surrounding neuritic plaques for patients with Alzheimer's disease (Allore *et al.,* 1988; Van Eldik & Griffin, 1994). S100β transgenic mice are found to undergo astrocytosis and neurite proliferation, suggesting that an excess of S100β may be relevant to the neuropathology of these cognitive diseases (Reeves *et al.*, 1994).

Presumably, the mechanism by which S100B functions *in vivo* depends upon tightly regulated intra- and extracellular Ca^{2+} concentrations (Kligman & Marshak, 1985). Each S100β subunit has a relatively high affinity Ca^{2+}-binding site ($K_D = 10-50\ \mu M$) and a significantly reduced affinity site ($K_D = 200-500\ \mu M$) (Baudier *et al.,* 1986; Kligman & Hilt, 1988). NMR data and sequence homology between S100B and other Ca^{2+}-binding proteins have previously indicated that each S100β subunit has two helix−loop−helix Ca^{2+}-binding domains known as EF-hands (Figure 1; Kretsinger, 1980; Kligman & Hilt, 1988; Strynadka & James,

† This work was supported in part by National Institutes of Health Grants R29GM52071 and S10RR10441 (to D.J.W.) and by SRIS and DRIF funding from the State of Maryland (to D.J.W.).

‡ Atomic coordinates of 20 apo-S100B structures and the associated restraints have been deposited with the Brookhaven Protein Data Bank under the file name 1SYM.

* To whom correspondence should be addressed: phone (410) 706-4354; FAX (410) 706-0458.

§ University of Maryland School of Medicine.

|| Present address: Department of Chemistry, The College of Wooster, Wooster, OH 44491.

⊥ The National Magnetic Resonance Facility at Madison.

Howard Hughes Medical Institute and University of Maryland Baltimore County.

□ Present address: Laboratory of Chemical Physics, Building 5, National Institute of Diabetes and Digestive and Kidney Diseases, National Institutes of Health, Bethesda, MD 20892-0520.

⊗ Abstract published in *Advance ACS Abstracts,* August 15, 1996.

[1] Abbreviations: βME, β-mercaptoethanol; DGSA, distance geometry-simulated annealing; EDTA, ethylenediaminetetraacetic acid; HOHAHA, homonuclear Hartmann−Hahn; GARP, globally optimized alternating-phase rectangular pulses; HMQC, heteronuclear multiple-quantum coherence; HSQC, heteronuclear single-quantum coherence; MARCKS, myristoylated alanine-rich kinase C substrate protein; NMR, nuclear magnetic resonance; NOESY, nuclear Overhauser effect spectroscopy; PKC, protein kinase C; RMSD, root mean square difference; ROESY, rotating frame Overhauser effect spectroscopy; S100β, a subunit of dimeric S100B; S100B($\beta\beta$), dimeric S100B with noncovalent interactions at the dimer interface; S100B($\beta-\beta$), dimeric S100B with disulfide bonds at the dimer interface; SLR, shaped radio-frequency pulse developed by Shinnar and LeRoux; TPPI, time-proportional phase incrementation; Tris-HCl, tris(hydroxymethyl)-aminomethane hydrochloride; TSP, sodium 3-(trimethylsilyl)propionate-*2,2,3,3-d*$_4$.

S0006-2960(96)01222-6 CCC: $12.00

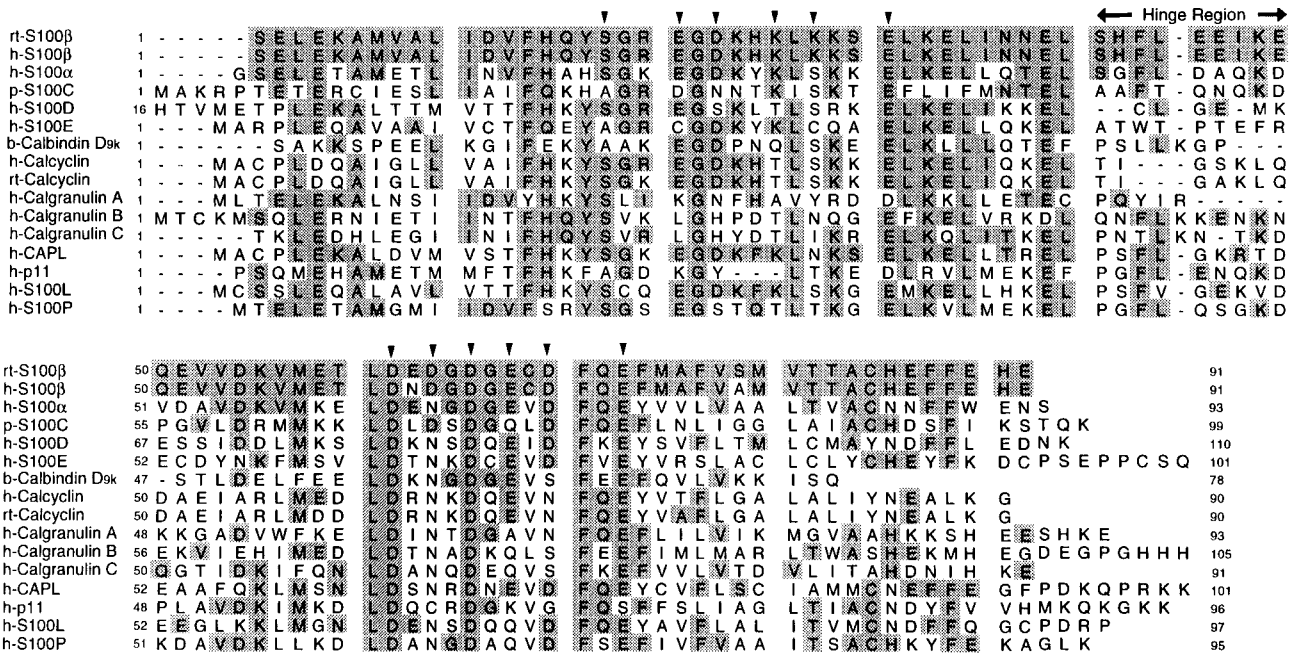

FIGURE 1: Amino acid sequence of S100β aligned with the sequences of other S100 proteins. The highlighted regions show sequence homology as determined by the Fassman 64 protocol in the program SeqVu (Gardner, 1995). Residues that coordinate Ca^{2+} are indicated by arrows at the X, Y, Z, −Y, −X and −Z sites, respectively. The first 15 residues of h-S100D are MPAAWILWAHSHSEL, and the final 9 residues of human calgranulin B are KPGLGEGTP. The prefixes are as follows: rt, rat; h, human; and p, porcine. The hinge region (loop II) and the C-terminal loop (loop IV) contain the least amount of sequence homology within the S100 protein family (Kligman & Hilt, 1988).

1989; Amburgey *et al.*, 1995). While the C-terminal EF-hand contains 12 residues as expected for a typical EF-hand, the N-terminal EF-hand contains 14 residues as expected for a pseudo EF-hand (ψ EF-hand) or S100-hand (Strynadka & James, 1989; Amburgey *et al.*, 1995). Upon binding Ca^{2+}, S100B undergoes a conformational change thought to promote its interaction with a variety of target proteins (Donato, 1991; Kligman & Hilt, 1988; Zimmer *et al.*, 1995; Hilt & Kligman, 1991). S100B target proteins include substrates of protein kinase C (PKC) such as MARCKS (Patel *et al.*, 1983; Patel & Kligman, 1987; Albert *et al.*, 1984), τ protein (Baudier *et al.*, 1987; Baudier & Cole, 1988a,b), p53 (Baudier *et al.*, 1992), and neuromodulin (Lin *et al.*, 1994; Sheu *et al.*, 1994). Interestingly, the loop which connects the two EF-hands in an S100β subunit, known as the hinge region, is postulated to be involved in binding target proteins on the basis of its lack of sequence homology to the hinge region of other S100 proteins (Figure 1; Kligman & Hilt, 1988).

S100B exists in solution as a dimer which, depending on conditions, is held together by noncovalent forces, S100B($\beta\beta$), or by disulfide bonds, S100B($\beta-\beta$) (Drohat *et al.*, 1996; D. B. Zimmer, T. L. Hall, A. Landar, E. H. Cornwall, J. J. Correia, A. C. Drohat, and D. J. Weber, unpublished observations). The cysteine residues of S100B are presumably reduced in the cytosol where the reduction potential is low, and the reduced form of S100B, S100B($\beta\beta$), is known to regulate fructose-1,6-bisphosphate aldolase and PKC *in vitro* (Zimmer *et al.*, unpublished observations; Wilder & Weber, 1996). Whereas, disulfide-linked S100B, S100B($\beta-\beta$), is presumably favored in extracellular environments, and it is known to modulate extracellular activities such as neurite extension (Kligman & Hilt, 1988). Many potential intra- and extracellular roles for S100B($\beta\beta$) and S100B($\beta-\beta$) have recently been discovered including enzyme regulation, intercellular communication, cell growth, cell structure, energy metabolism, contraction, and intracellular signal transduction [for reviews see Donato (1991), Kligman and Hilt (1988), Zimmer *et al.* (1995), and Schäfer and Heizmann (1996)].

To further characterize this important Ca^{2+}-binding protein, we have determined the structure of apo-S100B($\beta\beta$) in solution using data from a series of multidimensional NMR experiments. In the absence of Ca^{2+}, each S100β subunit contains two highly-structured helix−loop−helix Ca^{2+}-binding domains. In a manner similar to other Ca^{2+}-binding proteins, the two Ca^{2+}-binding domains are brought into close proximity by a short, two-stranded, antiparallel β-sheet (Amburgey *et al.*, 1995) and by significant hydrophobic interactions between the four α-helices. The overall conformation of the pseudo-EF-hand is similar to that of the pseudo-EF-hands in apo-calbindin D_{9k} and apo-calcylin. Whereas, the C-terminal EF-hand of apo-S100β differs significantly in conformation from EF-hands of apo-calbindin D_{9k}, apo-calmodulin, and apo-calcylin. This difference results from a novel orientation of helix III relative to helices I, II, and IV in each apo-S100β subunit. The structure of dimeric apo-S100B($\beta\beta$) exhibits an extensive hydrophobic core and a very highly charged solvent-exposed surface, consistent with its high solubility and stability *in vitro*. A preliminary abstract of this work has been published (Drohat *et al.*, 1996).

MATERIALS AND METHODS

NMR Sample Preparations. Isotopically enriched compounds including uniformly labeled [^{13}C]glucose (>99%) and $^{15}NH_4Cl$ (>99%) were purchased from Cambridge Isotope Laboratories (Woburn, MA). Unlabeled, ^{15}N-labeled, and ^{13}C,^{15}N-labeled apo-S100B($\beta\beta$) protein samples were prepared and purified (>98%) under reducing conditions using methods described previously (Amburgey *et al.*, 1995).

Unless otherwise stated, conditions for the 1.5−3.0 mM S100B($\beta\beta$) NMR samples were pH 6.5, 0.1 mM EDTA, 0.34 mM NaN_3, 2−10 mM βME, 5−10% D_2O, 6−10 mM Tris-HCl-d_{11}, and sufficient NaCl (17−20 mM) to give an ionic strength of 25 mM at 37 °C. An asymmetrically labeled NMR sample, with one ^{13}C,^{15}N-labeled subunit and one unlabeled subunit, was used to distinguish intra- from intermolecular NOE correlations (NOEs). This sample was prepared by mixing equal volumes of 3.0 mM unlabeled S100B($\beta\beta$) and 3.0 mM ^{13}C,^{15}N-labeled S100B($\beta\beta$) and incubating at 45 °C for 2 h, followed by two rounds of lyophilization and resuspension in 99.99% D_2O, to give 1.5 mM asymmetrically labeled dimer. S100B($\beta\beta$) NMR samples were tested for their ability to inhibit protein kinase C (PKC) dependent phosphorylation of a 22-residue peptide derived from the tumor suppressor protein, p53, as previously described (Wilder & Weber, 1996). After prolonged NMR experiments at 37 °C, no significant change (<5%) in PKC inhibition was observed.

NMR Spectroscopy. Table 1 lists the NMR experiments necessary to determine the solution structure of apo-S100B($\beta\beta$). NMR data were collected with Bruker DMX500, Bruker DMX600, and General Electric OMEGA-PSG600 NMR spectrometers, each equipped with at least three frequency channels, a triple resonance probe head, and pulsed field gradient capabilities. Unless otherwise stated, a 1 s relaxation delay was used, and quadrature detection in the indirect dimensions was obtained with States−TPPI phase cycling (Marion *et al.*, 1989). For most experiments, initial delays in the indirect dimensions were set to give zero- and first-order phase corrections of 90° and −180°, respectively (Bax *et al.*, 1991). Data were processed on Silicon Graphics workstations using the programs FELIX 2.3 (Biosym Technologies, Inc.) and nmrPipe (Delaglio *et al.*, 1995). Time−domain data in the indirect dimensions were extended by no more than one-third using standard linear prediction routines (Zhu & Bax, 1992), except for data from the ^1H−^{13}C constant-time HSQC (CT-HSQC) which was extended 2-fold using mirror-image linear prediction (Zhu & Bax, 1990). All proton chemical shifts are reported with respect to the H_2O or HDO signal, taken as 4.658 ppm relative to external TSP (0.0 ppm) at 37 °C. The ^{13}C and ^{15}N chemical shifts were indirectly referenced using the following ratios of the zero-point frequencies at 37 °C: 0.10132905 for ^{15}N to ^1H and 0.25144953 for ^{13}C to ^1H (Live *et al.*, 1984; Spera & Bax, 1991; Edison *et al.*, 1994).

Unlabeled S100B($\beta\beta$) in H_2O (10% D_2O) or D_2O (>99%) was used to record two-dimensional (2D) NOESY (Jeener *et al.*, 1979) and ROESY (Kessler *et al.*, 1987) experiments at 600 MHz. Low-power presaturation of the water signal during the 1.2 s relaxation delay was used to suppress H_2O and HDO resonances. The 2D NOESY experiments were recorded with mixing times between 50 and 300 ms, and the 2D ROESY experiment was recorded using a 90 ms spin−lock sequence with an average radio-frequency field strength of 2.8 kHz (Table 1; Kessler *et al.*, 1987). A 2D clean-HOHAHA (Bax & Davis, 1985) was collected for apo-S100B($\beta\beta$) in H_2O with a 70 ms spin−lock time.

Uniformly ^{15}N-enriched apo-S100B($\beta\beta$) was used to collect a 2D ^1H−^{15}N HMQC-J (Kay & Bax, 1990), a 3D ^{15}N-edited NOESY-HSQC (Kay *et al.*, 1989) with a 100 and a 200 ms mixing time, and a 3D ^{15}N,^{15}N-edited HMQC-NOESY-HMQC (Ikura *et al.*, 1990) with a 100 ms mixing time (Table 1). In the 3D NOESY experiments, presaturation of the H_2O and HDO resonances was performed by repeating a 10 ms phase-ramped SLR shape pulse (Shinnar *et al.*, 1989a,b) during the relaxation delay, and the residual solvent signal was further suppressed by convolution of the time domain data during processing (Marion *et al.*, 1989). Decoupling of ^{15}N was achieved by WALTZ-16 or GARP modulation (Shaka *et al.*, 1983, 1985). The HMQC-J was collected with a purge pulse prior to acquisition to eliminate phase distortions in the f_2 dimension (Kay & Bax, 1990).

A uniformly ^{13}C,^{15}N-labeled apo-S100B($\beta\beta$) sample was used to collect a 2D ^1H−^{13}C CT-HSQC (Vuister & Bax, 1992), a 3D ^{13}C-edited NOESY-HSQC (Muhandiram *et al.*, 1993b), a 4D ^{13}C,^{15}N-edited NOESY (Muhandiram *et al.*, 1993a), and a 4D ^{13}C,^{13}C-edited HMQC-NOESY-HSQC (Vuister *et al.*, 1993) using the parameters listed in Table 1. The 3D and 4D NOESY experiments were each collected with a 100 ms mixing time and a 0.9 s relaxation delay.

Table 1: Parameters for NMR Experiments[a]

		parameters[b]			
experiment	dim	nucl	time pts	freq pts	acq time (ms)
2D NOESY	t_1	^1H	384	2048	53.0
	t_2	^1H	2048	2048	254
2D ROESY	t_1	^1H	384	2048	53.0
	t_2	^1H	2048	2048	254
2D ^{13}C-filtered NOESY[c]	t_1	^1H	512	2048	66.6
	t_2	^1H	2048	2048	266
2D HMQC-J	t_1	^{15}N	512	2048	207
	t_2	^1H	512	2048	72.5
2D CT-HSQC[d]	t_1	^{13}C	83	512	16.6[e]
	t_2	^1H	1024	2048	146[f]
3D ^{15}N-edited NOESY HSQC	t_1	^1H	128	512	15.4
	t_2	^{15}N	32	64	12.8
	t_3	^1H	512	512	143[g]
3D ^{15}N,^{15}N-edited NOESY	t_1	^{15}N	64	128	40.5[h]
	t_2	^{15}N	32	128	20.2[h]
	t_3	^1H	256	512	63.5[g]
3D ^{13}C-edited NOESY[d]	t_1	^1H	128	256	21.2
	t_2	^{13}C	64	128	20.2
	t_3	^1H	1024	1024	139
3D ^{13}C-edited, ^{13}C-filtered NOESY[c]	t_1	^1H	120	512	20.0
	t_2	^{13}C	39	128	4.3[i]
	t_3	^1H	512	1024	61.0
4D ^{13}C,^{15}N-edited NOESY[d]	t_1	^{13}C	16	64	5.3[j]
	t_2	^1H	64	128	16.0[k]
	t_3	^{15}N	16	32	9.6
	t_4	^1H	384	1024	64.0[g]
4D ^{13}C,^{13}C-edited NOESY[d]	t_1	^{13}C	18	64	6.0[j,l]
	t_2	^1H	64	128	14.2[m]
	t_3	^{13}C	16	32	5.3[j,l]
	t_4	^1H	384	1024	63.9[m]

[a] Data was collected in H_2O at 600.13 MHz for ^1H unless otherwise noted. [b] Number of points given in the time dimension is complex. Number of points in the frequency dimension of processed spectra is real. The carrier frequencies were 4.658, 38.4, and 118.0 ppm for ^1H, ^{13}C, and ^{15}N nuclei, respectively, unless otherwise stated. [c] Data were collected on a sample in >99% D_2O. [d] Data were collected at 500.13 MHz for ^1H. [e] The carrier frequency for this ^{13}C dimension was 128.4 ppm for optimal detection of aromatic ^{13}C resonances. [f] The carrier frequency for this ^1H dimension was 7.00 ppm for the optimal detection of aromatic ^1H resonances. [g] The carrier frequency for this ^1H dimension was 8.70 ppm at the center of the amide proton region. [h] The ^{15}N carrier frequency was 117.0 ppm. [i] The ^{13}C carrier frequency was 40.4 ppm. [j] Since the sweep width in the ^{13}C dimension is 24.0 ppm, a significant number of resonances are folded. [k] The ^1H carrier frequency was set to 3.80 ppm. [l] The ^{13}C carrier frequency was 66.4 ppm. [m] The ^1H carrier frequency was 4.40 ppm.

Additional pulsed field gradients were used to purge undesired transverse magnetization (Bax & Pochapsky, 1992), and decoupling of ^{15}N and ^{13}CO using GARP and compensated SEDUCE-1 decoupling sequences were used, respectively (Shaka *et al.*, 1985; McCoy & Mueller, 1992). The CT-HSQC was acquired in H_2O with parameters optimized for detecting aromatic resonances as previously described (Abeygunawardana *et al.*, 1995).

Finally, the asymmetrically labeled S100B($\beta\beta$) NMR sample was used to collect a 2D $^{13}C(f_1, f_2)$ double-half-filtered NOESY (Folkers *et al.*, 1993; Starich, 1995) and a 3D ^{13}C-edited,^{13}C-filtered HMQC-NOESY comprising a conventional HMQC-NOESY concatenated with a ^{13}C filter prior to detection (Starich, 1995). Each was collected with a 150 ms mixing time, with pulsed field gradients for artifact suppression (Bax & Pochapsky, 1992), and with decoupling of ^{13}C achieved using GARP modulation (Shaka *et al.*, 1985).

NMR-Derived Restraints and Structure Calculations. NOE cross-peaks were classified on the basis of intensity as either strong, medium, weak or very weak, and assigned distance restraints with lower bounds of 1.8 Å and upper bounds of 2.7 (2.9 for H_N), 3.3 (3.5 for H_N), 5.0, and 6.0 Å, respectively (Clore *et al.*, 1986). Pseudo-atom corrections were added to the upper limit of restraints for degenerate methyl, methylene, and aromatic ring protons (Clore *et al.*, 1987; Wüthrich, 1986), and an additional 0.5 Å was added to the upper limit of restraints for methyl protons to account for the apparent higher intensity of methyl resonances (Clore *et al.*, 1987). Only distance restraints useful for the structure determination were incorporated, thus excluding NOEs between geminal protons or between vicinal methylene protons. Weak and very weak NOEs were used as restraints only when reciprocal NOEs with similar intensities were observed. NOEs that were suspected of having spin diffusion contributions to their intensity were confirmed by checking their sign and intensity in the 2D ROESY experiment, which was particularly important for analyzing intraresidue NOEs between amide and side-chain protons. Amburgey *et al.* (1995) previously found that 14 residues of apo-S100β exhibited multiple amide proton resonances for a single residue (S1, L3, E4, K5, A6, V8, L10, F14, S41, H42, F43, L44, E45, and E46) but that variations in the side-chain resonances of these residues were no greater than the digital resolution of the data. Accordingly, distance restraints for these residues were included only when a given NOE correlation was observed with similar intensity for each multiple amide proton resonance. Few differences were actually observed between the multiple amide proton resonances, and none were observed between the few existing multiple side-chain resonances, indicating that the structural variation about these residues is quite small. Backbone dihedral angle (ϕ) restraints, based on NMR-derived three-bond coupling constants ($^3J_{HN\alpha}$), were included with ranges of $\phi = -60° \pm 20°$ for $^3J_{HN\alpha} < 6$ Hz, and $\phi = -120° \pm 30°$ for $^3J_{HN\alpha} \geq 7.5$ Hz (Clore *et al.*, 1987). On the basis of secondary structural analysis and amide proton exchange rates determined previously (Amburgey *et al.*, 1995), hydrogen bond restraints were included with limits of 1.5−2.8 and 2.4−3.5 Å for the H to O and N to O distances, respectively.

Determination of the apo-S100β subunit structure preceded structure determination of the dimer and employed only unambiguous intramolecular NOEs and coupling constants as restraints. The hybrid distance geometry−simulated annealing (DGSA) protocol of the program X-PLOR 3.1 (Brünger, 1992) was used to calculate apo-S100β structures on a Silicon Graphics INDIGO2 workstation. The distance and dihedral angle restraints were incorporated using a square-well potential with 50 and 200 kcal/(mol·Å^2) force constants, respectively. The structures were then refined with the simulated annealing refinement protocol in X-PLOR 3.1, which incorporated hydrogen bond restraints. This process yielded low-energy apo-S100β subunit structures with no distance violations exceeding 0.5 Å and no dihedral violations exceeding 5°. The structures were also determined without H-bond restraints, and no significant change in the structure was observed.

Determination of the apo-S100B($\beta\beta$) dimer structure started with duplication of the coordinates from the lowest energy apo-S100β subunit structure. The resulting two subunit structures were then randomly separated and subsequently docked in a configuration consistent with several unambiguous intermolecular NOE correlations, using the graphics program CHAIN (Sack, 1988). Coordinates from the docked structure were used for initial structure determinations of the dimer, which included restraints for all of the unambiguous inter- and intramolecular NOE correlations. The dimer structure was refined in an iterative manner whereby preliminary structural models were used to assign additional NOE restraints. A total of 60 structures were then determined from randomized coordinates, incorporating all (2672) distance and (88) dihedral angle restraints, using the standard X-PLOR 3.1 protocols of substructure embedding and regularization, full-structure hybrid distance geometry−simulated annealing, and simulated annealing refinement (Table 2). The simulated annealing refinement included potential energy terms for noncrystallographic (NCS) and distance symmetry restraints with force constants of 100 and 1 kcal/(mol·Å^2), respectively, as described previously for other symmetric dimers (Nilges, 1993). This procedure yielded 20 apo-S100B($\beta\beta$) structures which had no NOE violations exceeding 0.2 Å, no dihedral violations exceeding 4°, low RMSDs from the experimental restraints and ideal covalent geometry, and low RMSDs from the mean structure. An additional 20 structures were determined with the same protocol but excluding H-bond restraints, and the low energy group of these 20 structures exhibited no significant change from those determined with H-bond restraints (Table 2). All color illustrations were produced with the graphics program MIDAS (Ferrin *et al.*, 1988).

RESULTS

Assignment of Aromatic Side-Chain Resonances. The complete sequence-specific resonance assignments for the tyrosine and seven phenylalanine residues per S100β subunit were critically important for the structure determination of apo-S100B($\beta\beta$) since a large number of intra- and intermolecular NOE correlations were observed to its aromatic protons. The eight aromatic ^1H spin systems were tentatively assigned using standard methods (Wüthrich, 1984), and the corresponding ^{13}C resonances were obtained using data from a ^{13}C-edited $^1H-^{13}C$ CT-HSQC experiment optimized for detecting aromatic resonances. The three $^1H-^{13}C$ correlations per ring system were assigned specific positions (δ, ϵ, ζ) by comparing relative NOE intensities observed in the

Table 2: NMR-Derived Restraints and Statistics of NMR Structures[a]

structural statistic	⟨20⟩	best
RMSDs from exptl distance restraints (Å) [b]		
all distance restraints (2672)	0.014 ± 0.002	0.012
intraresidue (348)	0.019 ± 0.003	0.017
sequential ($\|i-j\|=1$) (714)	0.014 ± 0.002	0.012
medium range ($1<\|i-j\|\leq 5$) (842)	0.013 ± 0.002	0.013
long range ($\|i-j\|>5$) (388)	0.009 ± 0.003	0.009
intermolecular (172)	0.011 ± 0.004	0.012
hydrogen bonds (208)	0.008 ± 0.004	0.004
max violation for distance restraint (Å)[c]	0.137 ± 0.029	0.121
RMSDs from exptl dihedral angle restraint (deg)[b]	0.313 ± 0.140	0.378
max violation for dihedral angle restraint (deg)[c]	1.41 ± 0.72	1.51
RMSDs from idealized covalent geometry		
bonds (Å)	0.0015 ± 0.0002	0.0015
angles (deg)	0.2410 ± 0.0020	0.2338
impropers (deg)	0.2237 ± 0.0142	0.2485
X-PLOR potential energies (kcal/mol)		
E_{total}	116 ± 19.7	106
E_{bonds}	7.10 ± 1.31	6.30
E_{angle}	47.3 ± 7.75	44.3
$E_{improper}$	12.6 ± 1.53	14.2
E_{repel}	23.5 ± 6.55	20.6
E_{NOE}	24.6 ± 5.44	19.8
E_{cdih}	0.63 ± 0.53	0.76
E_{ncs}	0.08 ± 0.06	0.05
Lennard-Jones potential energy (kcal/mol)[d]	−490 ± 38.0	−514
RMSDs of 20 structures (Å)	**relative to mean**	**pairwise**
backbone in secondary structure[e]	0.38 ± 0.05	0.55 ± 0.07
all backbone residues (N, C_α, C′)[f]	1.04 ± 0.11	1.50 ± 0.17
all heavy atoms	1.62 ± 0.14	2.35 ± 0.21
all backbone including structures without H-bonds[g]	1.07 ± 0.12	1.54 ± 0.19
all heavy including structures without H-bonds[g]	1.66 ± 0.14	2.39 ± 0.22

[a] ⟨20⟩ are the ensemble of 20 low-energy simulated annealing (SA) structures. The best of these 20 was chosen on the basis of its quality as measured by the statistics given in this table and as discussed in the text. For the ⟨20⟩, values shown are mean ± standard deviation. [b] The force constants of the target functions employed in the refinement were as follows: 1000 kcal·mol^{-1}·Å^{-2} for bond lengths, 500 kcal·mol^{-1}·rad^{-2} for angles and improper torsions, 4 kcal·mol^{-1}·Å^{-4} for the quartic van der Waals (vdw) repulsion term (hard sphere effective vdw radii set to 0.75 times their value in the CHARMM parameters), 50 kcal·mol^{-1}·Å^{-2} for experimental distance restraints, 200 kcal·mol^{-1}·rad^{-2} for the (ϕ) dihedral angle restraints, 100 kcal·mol^{-1}·Å^{-2} for the non-crystallographic symmetry restraints, and 1 kcal·mol^{-1}·Å^{-2} for the distance symmetry restraints. [c] The maximum violation in any of the ensemble of 20 structures was 0.186 Å for distance restraints and 3.54° for dihedral angle restraints. [d] The Lennard-Jones van der Waals energy was calculated using the CHARMM parameters and was not employed in any stage of the structure determination. [e] Calculation included the backbone heavy atoms (C_α, N, C′) in the four helices and the two β-strands per subunit (E2−Y17, K26−K28, K29−N38, Q50−D62, E67−D69, and F70−A82). [f] Calculation included *all* backbone residues including many in the loop regions that have a low number of restraints. [g] Calculated for an ensemble of 24 structures, four of which were determined without any H-bond distance restraints using the same protocol as for the 20 structures determined with H-bond distance restraints.

2D NOESY, 3D ^{15}N-edited NOESY, and the 4D ^{13}C,^{13}C-edited NOESY experiments. The sequence-specific assignment of these ring systems was confirmed by numerous NOE correlations to previously assigned resonances (Wüthrich, 1984). Assignment of the remaining unassigned aliphatic side chains was also completed. These assignments together with those of Amburgey *et al.* (1995) complete the sequence-specific assignment of all backbone and side-chain resonances observable for rat apo-S100β.[2]

Assignment of Intra- and Intermolecular NOE Correlations. Chemical shift degeneracy attributed to the high α-helical content of apo-S100B($\beta\beta$) (Amburgey *et al.*, 1995) and ambiguity arising from its symmetric dimer interface significantly complicated the assignment of NOE correlations. Therefore, 2D and 3D NOESY spectra were supplemented by 4D ^{13}C,^{15}N-edited NOESY, 4D ^{13}C,^{13}C-edited NOESY, and 3D ^{13}C-filtered NOESY spectra to assign over 50% of the long-range and intermolecular NOE correlations on the basis of chemical shift values alone (Table 1; Figures 2−4). NOEs observed in the 3D ^{13}C-edited and 4D ^{13}C,^{13}C-edited NOESY experiments were classified as intramolecular if no corresponding cross-peaks were found in the 2D ^{13}C-filtered NOESY and/or 3D ^{13}C-edited,^{13}C-filtered HMQC-NOESY spectra. In fact, the majority of these intramolecular NOE correlations were assigned by comparing data from the 4D ^{13}C,^{13}C-edited NOESY and the 3D ^{13}C-filtered NOESY spectra, as shown for the δ-methyl protons of L60 in Figure 4. Similarly, intermolecular NOEs observed in the ^{13}C-filtered NOESY experiments were unambiguously assigned using data from the 4D ^{13}C,^{13}C-edited NOESY experiment. Several NOE correlations were determined to have both intra- and intermolecular contributions, based primarily on relative peak intensities in the 4D ^{13}C,^{13}C-edited NOESY and 3D ^{13}C-edited,^{13}C-filtered NOESY experiments and supported by preliminary structural models. These and other ambiguous NOE correlations were assigned in a conservative manner and were used only in the later stages of the structure determination as a more detailed understanding of the dimer interface emerged.

[2] The ^{1}H and ^{13}C chemical shift values for aromatic and other previously unassigned side-chain resonances of apo-S100B($\beta\beta$) were added to a table of chemical shift values for this protein currently in the BioMagResBank chemical shift data bank located at the University of Wisconsin at Madison.

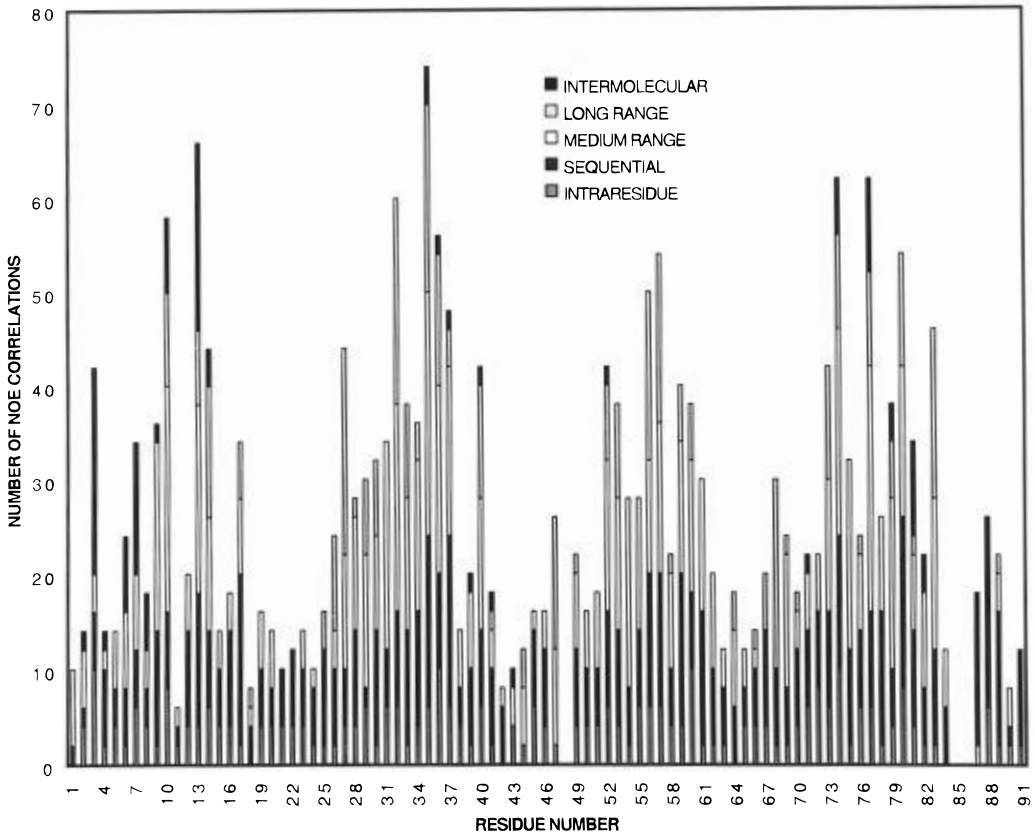

FIGURE 2: Distribution of NOE-derived restraints (by residue) used to determine the structure of apo-S100B($\beta\beta$). The number of restraints shown for each residue includes those from both subunits.

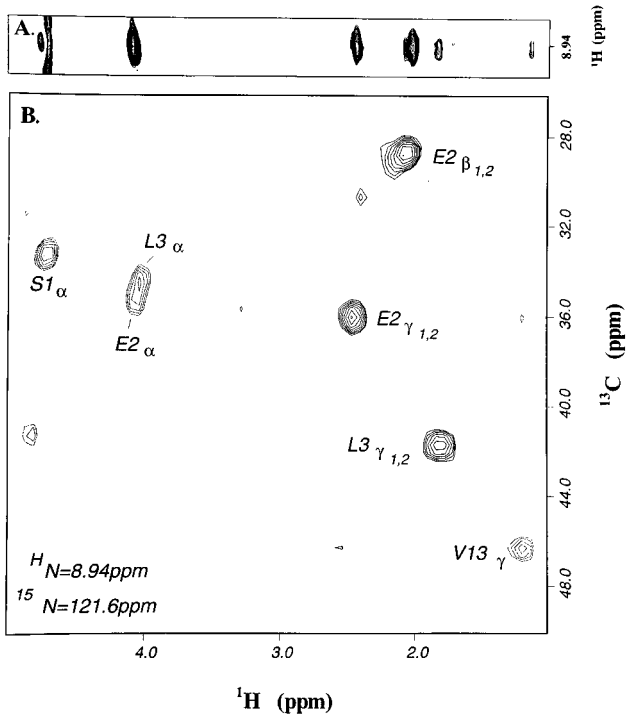

FIGURE 3: Spectra from the 4D ^{13}C,^{15}N-edited NOESY and 2D ROESY illustrating an *inter*molecular NOE correlation in helix I. (A) A strip from the 2D ROESY spectrum showing NOE correlations to the L3 amide proton and (B) the corresponding plane from the 4D ^{13}C,^{15}N-edited NOESY. The NOE correlation from the L3 amide proton to the methyl protons of V13 must be intermolecular since L3 and V13 are at opposite ends of helix I (see text).

At an early stage in the NOE assignment process it became clear that helices I and IV were an integral part of the dimer interface in apo-S100B($\beta\beta$). Initial evidence for the involvement of helix I was found in the 4D ^{13}C,^{15}N-edited NOESY spectra, where an unambiguous NOE correlation between the amide proton of L3 and the methyl protons of V13 was identified (Figure 3). Spin diffusion, though unlikely at such a distance, was ruled out as a contributor to this NOE correlation since its magnitude was similar in the 2D ROESY spectrum (Figure 3). This NOE was classified intermolecular because of the physical impossibility of the N- and C-termini of helix I being close in space. The antiparallel alignment of helix I (subunit a) with helix I′ (subunit b) was confirmed by the identification of numerous additional intermolecular NOE correlations in the 2D ^{13}C-filtered, 3D ^{13}C-edited,^{13}C-filtered, and 4D ^{13}C,^{13}C-edited NOESY spectra. These include strong NOE correlations observed between the methyl protons of L3 and the methyl protons of L10 and V13. Numerous other intermolecular NOE correlations indicate that helices IV and IV′ are also antiparallel at the dimer interface. In total, 172 intermolecular NOE restraints (86 per subunit) involving residues in helix I (E2, L3, E4, A6, M7, V8, A9, L10, I11, V13, F14, and Y17), helix II (L35, I36, N37, E39, and L40), loop II (S41 and F43), helix III (V52), helix IV (F70, Q71, M74, A75, V77, M79, T81, and T82), and loop IV (F87, F88, and E89) define the dimer interface of apo-S100B($\beta\beta$) (Figure 2).

Structure Determination and Quality of the Structures. The structure determination of apo-S100B($\beta\beta$) incorporated 2464 NOE-derived distance restraints (13.5/residue), 88 (ϕ) dihedral angle restraints, and 208 H-bond restraints (Table 2) as described under Materials and Methods. Figure 5A shows the α-carbon superposition of the 20 low-energy structures which exhibit minimal van der Waals contacts, no distance restraint violations exceeding 0.2 Å, no dihedral

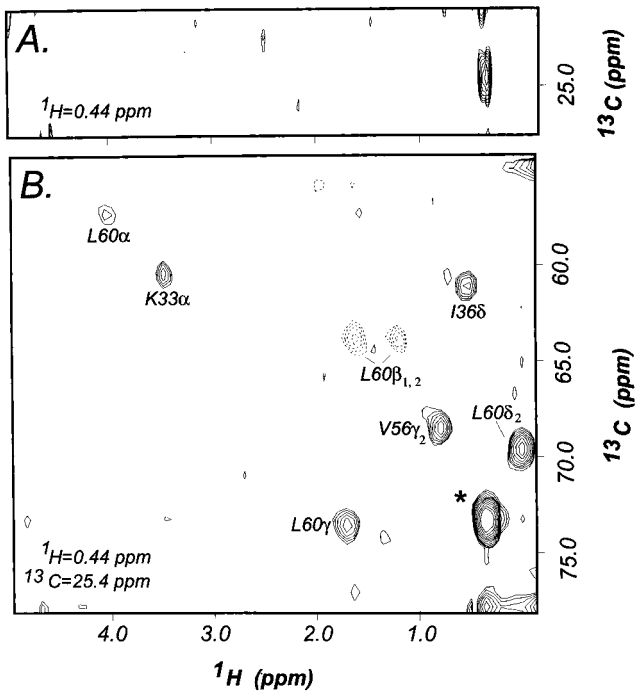

FIGURE 4: Spectra from the 4D ^{13}C,^{13}C-edited NOESY and the 3D ^{13}C-edited, ^{13}C-filtered HMQC-NOESY illustrating long-range *intra*molecular NOEs and lack of *inter*molecular NOEs to L60−δ_1CH$_3$ protons. (A) A ^{1}H−^{13}C strip from a plane (^{1}H = 0.44 ppm = L60−δ_1CH$_3$ chemical shift) of the 3D ^{13}C-edited,^{13}C-filtered HMQC-NOESY illustrates the lack of *inter*molecular NOE correlations to the δ_1CH$_3$ protons of L60. (B) Long-range *intra*molecular NOE correlations are observed in the corresponding plane (optimized for L60−δ_1CH$_3$ protons) from the 4D ^{13}C,^{13}C-edited NOESY. These NOEs demonstrate the interaction of residues in the C-terminus of helix III (L60) with residues in helix II (K33−Hα and I36−δCH$_3$). Contours with dashed lines represent NOE correlations folded an odd number of times, whereas contours with solid lines represent those folded an even number of times or not folded. The contour labeled with an asterisk is the autocorrelation peak.

angle violations exceeding 4°, and low RMSDs from the experimental restraints and from ideal covalent geometry (Table 2). Further, these 20 structures exhibit low RMSDs relative to their mean and low pairwise RMSDs (Table 2). Due to the significant number of experimental restraints and to the NCS and distance symmetry restraints employed during simulated annealing refinement, the RMSDs between S100β subunits for a given structure are negligible. The best of these 20 structures (Figure 5B) was chosen on the basis of its minimal values in the categories listed in Table 2. Additionally, a Ramachandran plot of backbone (ϕ,ψ) dihedral angles for the best apo-S100B($\beta\beta$) structure (Figure 6) shows that no residues are in the disallowed region, 69 residues (76%) are in most favored regions, 21 residues (23%) are in the additionally allowed regions, and the remaining residue is in the generously allowed region (Figure 6). Finally, the overall quality of the 20 apo-S100B-($\beta\beta$) structures, assessed by several protocols of the program PROCHECK (Laskowski *et al.*, 1993), is comparable to that of a well-defined 2 Å X-ray structure with an *R*-factor <20%.

Tertiary Structure of the Apo-S100β Subunits. Apo-S100B($\beta\beta$) is found to exist as a homodimer in solution composed of two symmetric apo-S100β subunits. As illustrated in Figure 5B, each subunit has two helix−loop−helix Ca^{2+}-binding domains known as EF-hands. The Ca^{2+}-binding loop in each EF-hand contains a short β-strand (K26−K28, β-strand I; E67−D69, β-strand II), and these β-strands form an antiparallel β-sheet as described previously (Amburgey *et al.*, 1995). This small β-sheet, together with extensive hydrophobic interactions between the four helices, brings the two Ca^{2+}-binding domains into close proximity as observed for other proteins containing EF-hands (Strynadka & James, 1989). The N-terminal pseudo EF-hand includes helix I (E2−S18), loop I (G19−K28), and helix II (K29−L40), while the C-terminal typical EF-hand comprises helix III (Q50−E62), loop III (D63−D69), and helix IV (F70−T82). The EF-hands are connected by loop II (S41−E49), known as the hinge region, and the C-terminal EF-hand is followed by loop IV (A83−E91), both of which lack homology with similar regions in other S100-family proteins.

The pseudo-EF-hand of each apo-S100B($\beta\beta$) subunit is found to be similar in conformation to the pseudo-EF-hands in apo-calbindin D$_{9k}$ and apo-calcyclin (Figure 7A; Table 3). Although many residues in helix I are involved in the dimer interface, intramolecular interactions typical of other Ca^{2+}-binding proteins are also observed. For example, C-terminal residues of helix I exhibit interactions with loop I (NOEs from Y17 and S18 to L27), with helix II (NOEs from V13 and Y17 to L35), and most extensively with the N-terminus of helix IV (NOEs from L10 to M74 and V77 and from F14 to F70 and F73). Residues of helix II exhibit extensive hydrophobic interactions with loop I (NOEs from L32 and L35 to L27), with the C-terminus of helix III (NOEs from K29, L32, K33, and I36 to M57 and L60), and with helix IV (NOEs from L32 to F73 and V77, from I36 to V77 and V80, and from L40 to V77 and V80). These interactions result in an interhelical angle for helices I and II of 132°, which is quite similar to that observed in apo-calbindin D$_{9k}$ (123°), apo-calmodulin (138°), and apo-calcyclin (126°) (Potts *et al.*, 1995; Skelton *et al.*, 1990; Kuboniwa *et al.*, 1995). The interhelical angles of helices I and IV (124°) and helices II and IV (−35°) for apo-S100β are also typical of these proteins in the apo-state (Table 3).

The C-terminal EF-hand of each apo-S100B($\beta\beta$) subunit is found to differ significantly from other EF-hands in regard to the position of helix III relative to helices I, II, and IV. The position of helix III is well defined by a large number of unambiguous NOE correlations. The N-terminal residues of helix III have extensive hydrophobic interaction with C-terminal residues of helix IV (NOEs from V52, V53, and V56 to M79, V80, and A83), and the C-terminal residues exhibit hydrophobic interactions with residues throughout helix II (NOEs from M57 and L60 to K29, L32, K33, and I36) (Figure 4). The resulting interhelical angle of helices III and IV ($\Omega_{3/4}$ = −142°) differs significantly from that known for other EF-hands in the apo- or Ca^{2+}-bound state (Table 3; Figure 7B). Specifically, it differs by 86° from $\Omega_{1/2}$ in the pseudo-EF-hand of apo-S100β ($\Omega_{1/2}$ = 132°), by ≥73° from the $\Omega_{1/2}$ or $\Omega_{3/4}$ of the EF-hands in apo-calcyclin, apo-calbindin, and apo-calmodulin ($\Omega_{1/2}$ and $\Omega_{3/4}$ range from 118° to 145°), and by ≥90° from the $\Omega_{1/2}$ or $\Omega_{3/4}$ for the Ca^{2+}-saturated EF-hands in calbindin D$_{9k}$ or calmodulin ($\Omega_{1/2}$ and $\Omega_{3/4}$ ranges from 84° to 128°). Similarly, the orientation of helix III in apo-S100B($\beta\beta$) provides an $\Omega_{1/3}$ of −20° and an $\Omega_{2/3}$ of −144°, which differ significantly from those of the apo- and Ca^{2+}-saturated forms of these EF-hand proteins as shown in Table 3.

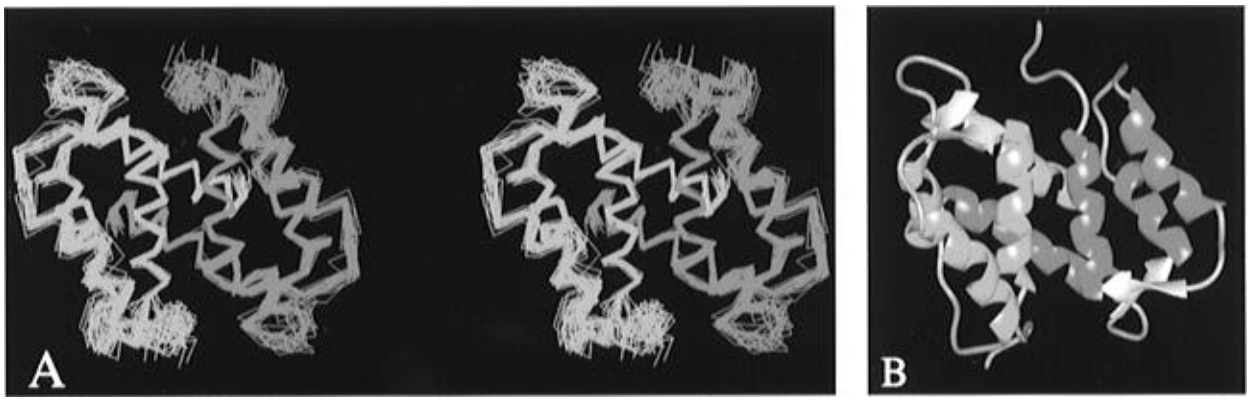

FIGURE 5: (A) Stereoview of the C_α superposition of 20 structures of apo-S100B($\beta\beta$), with the S100β subunits shown in different colors. The statistical quality of these structures is given in Table 2. (B) Ribbon diagram of apo-S100B($\beta\beta$) illustrating the X-type four-helix bundle (two pairs of crossing helices) at the dimer interface and the unicornate-type four-helix bundle (one helix forms a large angle with the others) within each subunit. The small β-sheet of each apo-S100β subunit (pink) and the loops (gray) are also shown.

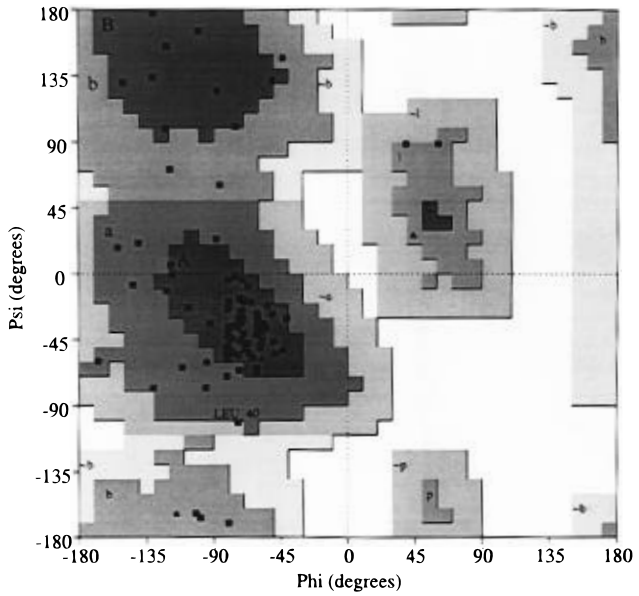

FIGURE 6: Ramachandran plot of the best apo-S100B($\beta\beta$) structure. Seventy-six percent of the residues fall in the most favored regions (A, B, and L), 23% are in the additionally allowed regions (a, b, l, and p), and the remaining 1% (residue) falls in the generously allowed region (~a, ~b, ~l, and ~p). Glycine residues are shown as triangles.

The hinge region (loop II) and the C-terminal loop of each apo-S100β subunit, also known as the variable loops, share the least amount of sequence homology with other S100 or EF-hand-containing proteins and are therefore suggested to be responsible for binding target proteins (Kligman & Hilt, 1988). Interestingly, these variable loops are proximal and form a surface which encompasses the C-terminal regions of helices II and IV, the N-terminal region of helix III, and regions of the other subunit (Figures 5 and 8). Residues in loop II share hydrophobic interactions with the C-terminus of helix IV (NOEs from F43 to T81 and from I47 to A83), and loop II therefore wraps around the C-terminal region of helix IV (Figures 5 and 8). Residues in loop IV (A83−E91) interact with the N-terminus of helix III (NOEs from A83 to V52 and V53) and with the N-terminus of helix IV′ and the C-terminus of helix I′ of the other subunit (Figure 5). It will be important to determine the location and conformation of the variable loops in the Ca^{2+}-bound state, since most of the target proteins that bind S100B($\beta\beta$) do so in a Ca^{2+}-dependent manner (Kligman & Hilt, 1988).

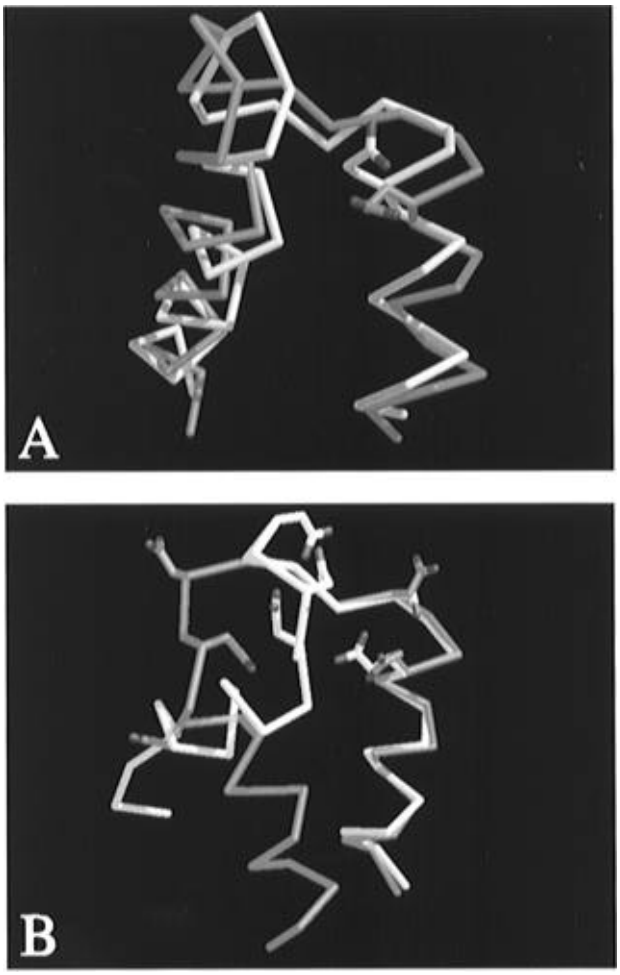

FIGURE 7: Comparison of the EF-hands of apo-S100B($\beta\beta$) and apo-calbindin D_{9k}. (A) Residues A6−L40 of the (N-terminal) pseudo-EF-hand in apo-S100β (blue) are superimposed (C_α) with the analogous residues, K5−F39, in the pseudo-EF-hand of calbindin (white). (B) Residues Q50−A83 from the (C-terminal) typical EF-hand in apo-S100B($\beta\beta$) (blue) are superimposed (C_α) with the homologous residues (L49−Q78) of the typical EF-hand in apo-calbindin D_{9k} (white). The overlay was performed by aligning residues 67−82 of apo-S100B($\beta\beta$) with residues 63−78 of apo-calbindin D_{9k}, which include the C-terminal β-strand and helix IV from each protein.

The tertiary structure of each apo-S100β subunit, resulting from both intra- and intermolecular interactions, is classified as a unicornate-type four-helical bundle (Harris *et al*., 1994).

Table 3: Interhelical Angles of EF-Hands in Ca^{2+}-Binding Proteins[a]

helices	apo-S100B($\beta\beta$)[b,c]	apo-calcyclin[d]	apo-calbindin[e]	apo-calmodulin[f]	Ca^{2+}-calmodulin[g]	Ca^{2+}-calbindin[h]
I−II	$132 \pm 4^{\perp}$	$126 \pm 27^{\perp}$	$123 \pm 3^{\perp}$	$138 \pm 2^{\perp}$ $(131 \pm 4)^{\perp}$	87 $(105)^{\perp}$	$128^{\perp}$
I−III	$-20 \pm 3^{\parallel}$	$-83 \pm 22^{\perp}$	$-109 \pm 9^{\perp}$	$-88 \pm 3^{\perp}$ $(-81 \pm 5)^{\perp}$	160 $(142)^{\parallel}$	$-113^{\perp}$
I−IV	$124 \pm 2^{\perp}$	$119 \pm 17^{\perp}$	$128 \pm 4^{\perp}$	$127 \pm 2^{\perp}$ $(142 \pm 5)^{\parallel}$	110 $(119)^{\perp}$	$120^{i,\perp}$
II−III	$-144 \pm 2^{\parallel}$	$144 \pm 15^{\parallel}$	$124 \pm 7^{\perp}$	$126 \pm 3^{\perp}$ $(141 \pm 5)^{\parallel}$	113 $(113)^{\perp}$	$113^{\perp}$
II−IV	$-35 \pm 1^{\parallel}$	$-16 \pm 10^{\parallel}$	$-34 \pm 4^{\parallel}$	$-47 \pm 2^{\perp}$ $(-30 \pm 5)^{\parallel}$	-45 $(-37)^{\perp}$	$-28^{i,\parallel}$
III−IV	$-142 \pm 3^{\parallel}$	$145 \pm 16^{\parallel}$	$118 \pm 8^{\perp}$	$130 \pm 3^{\perp}$ $(133 \pm 4)^{\perp}$	84 $(96)^{\perp}$	$126^{i,\perp}$

[a] Interhelical angles (Ω), defined as discussed below (footnote *b*), range from $-180°$ to $+180°$. Shown with each Ω is its classification as either parallel ($\parallel$) for $0° \leq |\Omega\ acute| \leq 40°$ or perpendicular ($\perp$) for $40° < |\Omega\ acute| \leq 90°$, as described (Harris *et al.*, 1994). [b] Interhelical angles for apo-S100B($\beta\beta$) were measured, similarly to Kuboniwa *et al.* (1995), as follows. Using the graphics program CHAIN (Sack, 1988), an S100β subunit was oriented such that (1) the two helices of interest (*i*,*j*) were in planes parallel to the screen, (2) the first helix (i) was in front of the second helix (j), and (3) the first helix (*i*) was aligned vertically (0°) with its N → C vector pointing upward. An imaginary vector aligned vertically (0°) with its tail at the N-terminus of the second helix (*j*) was rotated (by ≤180° clockwise or counterclockwise) until it aligned with the N → C vector of the second helix (*j*). This angle of rotation defined the interhelical angle Ω, with a clockwise rotation giving a positive Ω value and a counterclockwise rotation giving a negative Ω value. The low standard deviations of the Ω values measured for apo-S100B($\beta\beta$) show that the method is repeatable and that the structures are well converged. [c] Helices in apo-S100β are as follows: helix I (E2−S18), helix II (K29−L40), helix III (Q50−D62), and helix IV (F70−T82). [d] Helices in apo-calcyclin are defined in Potts *et al.* (1995) as follows: helix I (residues 4−16), helix II (residues 32−42), helix III (residues 53−62), and helix IV (residues 70−85). [e] Helices in apo-calbindin are defined in Skelton *et al.* (1995) as follows: helix I (residues 3−13), helix II (residues 25−35), helix III (residues 46−54), and helix IV (residues 63−72). [f] Helices in apo-calmodulin are defined in Kuboniwa *et al.* (1995) as follows: helix I (residues 6−18), helix II (residues 29−38), helix III (residues 45−54), and helix IV (residues 65−74). Interhelical angles for the third and fourth EF-hands in apo-calmodulin are listed in parentheses next to the analogous helices in the first and second EF-hands. These helices are defined in Kuboniwa *et al.* (1995) as follows: helix V (residues 83−91), helix VI (residues 102−111), helix VII (residues 118−127), and helix VIII (residues 139−145). [g] Taken from Babu *et al.* (1988). [h] Taken from Szebenyi *et al.* (1986). [i] The angle was taken from the center portion of the bent helix IV in calbindin as described in Szebenyi *et al.* (1986).

This motif, observed in a number of other proteins including T4 lysozyme, contains one helix at a large angle with the three other nearly parallel helices in the bundle (Harris *et al.*, 1994). In an apo-S100β subunit, helix I is nearly perpendicular to helices II and IV which are both nearly parallel to helix III (Figure 5; Table 3). This tertiary structure differs from the splayed-type four-helical bundle observed in the S100-family protein calbindin D_{9k}, in which the four helices around the bundle are perpendicular (Table 3; Harris *et al.*, 1994). Although conformational differences are apparent between apo-S100B($\beta\beta$) and apo-calcyclin (another S100-family protein), the calcyclin subunit also appears to adopt a unicornate-type four-helical bundle.

Quaternary Structure of Apo-S100B($\beta\beta$). The dimer interface of apo-S100B($\beta\beta$) is characterized by the antiparallel alignment of helices I (subunit a) and I′ (subunit b), the antiparallel alignment of helices IV (subunit a) and IV′ (subunit b), and the perpendicular association of these pairs of antiparallel helices to form an X-type four-helical bundle (Figure 5; Harris *et al.*, 1994). The X-type four-helical bundle motif, characterized by two pairs of crossing helices, has been observed as an element of larger structure in several proteins including a domain of 3-isopropylmalate dehydrogenase (Harris *et al.*, 1994). The symmetric apo-S100β subunits associate via extensive hydrophobic interactions involving helices I, II, and IV and loops II and IV from each subunit. Because many of the hydrophobic residues found to be involved in the dimer interface are highly conserved in S100 proteins (Figure 1), this may turn out to be a common mode of association for members of this Ca^{2+}-binding protein family, as previously suggested (Potts *et al.*, 1995; Krebs *et al.*, 1995). The conserved residues at the dimer interface of apo-S100B($\beta\beta$) include L3, A6, L10, I11, F14, Y17, L35, I36, L40, F43, F70, F73, V77, and F88, whereas several less conserved or nonconserved residues include M7, V8, A9, M74, T81, T82, and F87.

The majority of the hydrophobic interactions joining the two apo-S100β subunits are observed between residues of helix I and helices I′ and IV′. The antiparallel association of helices I and I′ is evidenced by many unambiguous intermolecular NOEs, including those from L3 to L10′ and V13′ (Figure 3) and from A6 to L10′. Interestingly, A6 and A9 (A6′ and A9′) are located near the crossing point of helices I and I′ and thus provide both hydrophobic interaction and low steric hindrance. The perpendicular association of helices I and IV′ is evidenced by unambiguous NOEs from L3 to F73′, M74′, and V77′ and by NOEs from M7 to M74′ and V77′. A small number of intermolecular NOE correlations are observed between the side chains of helices IV and IV′, including an NOE from T82 to F70. Residues of helix IV that participate in intermolecular hydrophobic interactions do so mostly with loop IV′ and helix I′ rather than helix IV′. Residues at the interface of helices IV and IV′ such as Q71, A75, S78, and T82 may serve to shield the hydrophobic core while providing low steric hindrance for the packing of the helices. Hydrophobic interactions at the dimer interface of apo-S100B($\beta\beta$) also include those between the N-terminus of helix I and the C-terminus of helix II′ (NOEs from L3 to L35′ and I36′) and loop II′ (NOEs from V8 to L40′ and F43′). The C-terminal variable loop plays an important role in the dimer interface via hydrophobic interaction with the N-terminus of helix IV′ (NOEs from F87 and F88 to F70′) and the C-terminus of helix I′ (NOEs from F87 and F88 to F14′).

Hydrophobic interactions for residues F14, F70, M74, and F88 at the dimer interface of apo-S100B($\beta\beta$) were also found for homologous residues in apo-calcyclin, and the dimer interface of each is similar in many respects; however, some differences are also observed (Potts *et al.*, 1995). The interhelical angle of helices IV and IV′ in apo-S100B($\beta\beta$) is $155 \pm 5°$, which is quite similar to that observed for calcyclin at $143 \pm 7°$. However, residues throughout helices I and I′ in apo-S100B($\beta\beta$) exhibit a large number of hydrophobic interactions resulting in an interhelical angle of $-165 \pm 4°$, and the N-terminus of helix I exhibits hydrophobic interaction with helices II′ and IV′, which appears to differ from apo-calcyclin (Potts *et al.*, 1995).

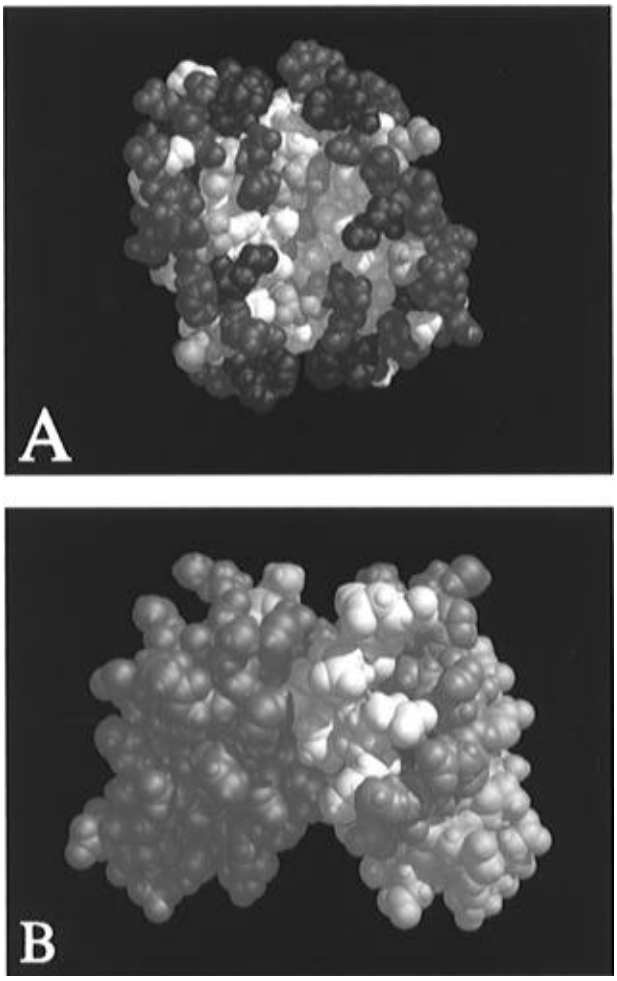

FIGURE 8: (A) Space-filling model of apo-S100B($\beta\beta$) showing basic residues (Arg, Lys, and His) in blue, acidic residues (Glu and Asp) in red, polar residues in purple, C68 and C84 of each subunit in yellow, and other residues in white. (B) Space-filling model of apo-S100B($\beta\beta$) with one subunit shown in blue and the other in yellow, loop II shown in gray, loop IV shown in white, and C84 shown in magenta.

DISCUSSION

Many previously observed characteristics of apo-S100B($\beta\beta$), including its thermal stability and high solubility, can be somewhat explained upon the examination of its three-dimensional structure. For example, 82 hydrophobic residues (45% of all residues) participate in a hydrophobic core that extends from the X-type four-helix bundle at the dimer interface into the unicornate-type four-helix bundle of each apo-S100β subunit (Figure 5). The presence of such extensive hydrophobic interaction may explain the stability of the apo-S100B($\beta\beta$) dimer ($K_D < 1\ \mu M$) in the absence of denaturants such as guanidinium chloride and sodium dodecyl sulfate (Zimmer *et al.*, unpublished observations). Additionally, the locations of C68 and C84 in this hydrophobic core may illustrate why these residues are not reactive with chemical modifying reagents in the absence of Ca^{2+} as observed previously (Baudier & Cole, 1988a,b). Finally, 76 charged residues (42% of all residues) and 24 polar residues (13% of all residues) cover the surface of apo-S100B($\beta\beta$), as shown in Figure 8A. The high percentage of hydrophilic residues on the surface of apo-S100B($\beta\beta$) readily explains its high solubility.

On the basis of sequence homology of S100β with other Ca^{2+}-binding proteins (Strynadka & James, 1989), it is predicted that the carboxylate oxygens of D61, D63, E65, and the backbone carbonyl oxygen of E67 coordinate Ca^{2+} in the X, Y, Z, and $-$Y positions, respectively. Presumably, the two carboxylate oxygens of E72 coordinate Ca^{2+} in a bidentate manner at the $-$Z and $-$Z′ positions as observed for other EF-hands (Strynadka & James, 1989).[3] This predicted coordination scheme would leave an opening at the $-$X position for a water ligand, as typically observed (Strynadka & James, 1989). This prediction is supported by results from laser-induced lanthanide luminescence spectroscopy which show that water molecules occupy two of the eight Eu(III) coordination sites in the C-terminal EF-hand of S100β, as previously observed in all four EF-hands of calmodulin (Chaudhuri *et al.*, 1996; Bruno *et al.*, 1992; W. D. Horrocks, personal communication).[4] Therefore, six sites are coordinated by residues from S100β, as found previously for calmodulin (Chaudhuri *et al.*, 1996; W. D. Horrocks, personal communication).

In calmodulin and other EF-hand-containing proteins it is known that the backbone structure of the Ca^{2+}-binding loop is remarkably similar in the apo- and Ca^{2+}-loaded states except at the $-$Z and $-$Z′ positions (Kuboniwa *et al.*, 1995). It is now generally recognized that the bidentate coordination of Ca^{2+} by a glutamate residue at the $-$Z and $-$Z′ positions triggers a global conformational change for these proteins (Kuboniwa *et al.*, 1995). However, when the C-terminal EF-hand of apo-S100β (residues 67$-$82) is superimposed (with backbone C_α) on the analogous region in apo-calbindin D_{9k} (residues 63$-$78), the alignment of the Ca^{2+}-coordinating ligands for both the side-chain and backbone atoms is significantly different in the X, Y, and Z positions, whereas they overlay fairly well in the $-$Y, $-$Z, and $-$Z′ positions (shown in Figure 7A). Thus, residues D61, D63, D65, and E72 at the X, Y, Z, $-$Z, and $-$Z′ positions, respectively, must significantly change their location upon the addition of Ca^{2+} in order to obtain the consensus EF-hand conformation in the Ca^{2+}-bound state. Support for a conformational change in the C-terminal EF-hand of S100B($\beta\beta$) upon the addition of a single equivalent of Ca^{2+} is provided by several biophysical studies, including NMR (Kligman & Hilt, 1988; Drohat *et al.*, 1995). We have observed large changes in chemical shift, line widths, and NOE correlations during Ca^{2+} titrations of S100B($\beta\beta$) (data not shown), although it is presently difficult to assess whether the conformational change involves movements of residues in the Ca^{2+}-binding loop, reorientation of helices, or both (Donato, 1988; Drohat *et al.*, 1995; work in progress).

Large changes in the conformation of the pseudo-EF-hand in apo-S100B($\beta\beta$) will probably not be observed upon binding Ca^{2+} since its structure is already quite similar to

[3] The nomenclature for an EF-hand identifies only six (X, Y, Z, $-$X, $-$Y, and $-$Z) of the seven possible Ca^{2+}-coordination sites (Strynadka & James, 1989), and we refer to the final coordination site as $-$Z′. Ligands to the $-$Z and $-$Z′ sites are generally provided by a glutamate residue at position 12 in the EF-hand via bidentate coordination (Strynadka & James, 1989).

[4] In solution, Eu(III) is known to coordinate nine ligands when the geometry is ideal, and a majority of these ligands are relatively small. However, several observations with Eu(III) indicate that it coordinates only eight ligands when it occupies EF-hands in parvalbumin and calmodulin (Horrocks, 1996; Cronce & Horrocks, 1992; Bruno *et al.*, 1992; Horrocks & Sudnick, 1981).

the analogous apo- and Ca^{2+}-loaded pseudo-EF-hand observed in calbindin D_{9k} (Skelton *et al.*, 1990). Thus, on the basis of sequence homology between the pseudo-EF-hands of S100β and calbindin D_{9k} (Szebenyi & Moffatt, 1986), it has been predicted that bidentate coordination of Ca^{2+} by the carboxylate oxygens of E31 in apo-S100B($\beta\beta$) at the −Z and −Z′ positions will occur (Amburgey *et al.*, 1995; Strynadka & James, 1989). The remaining five Ca^{2+} coordination sites were thought to be filled by a single water molecule at the −X position and backbone carbonyl oxygens from residues S18, E21, D23, and K26 at the X, Y, Z, and −Y positions, respectively. However, results from laser-induced lanthanide luminescence spectroscopy indicate that five (rather than six) sites of Ca^{2+} are coordinated by residues from the S100β subunit, which means that an additional water molecule is located in the Ca^{2+} coordination sphere (Chaudhuri *et al.*, 1996; W. D. Horrocks, personal communication). Because the carbonyl oxygen atoms of residues S18, E21, D23, K26, and the carboxylate oxygen atoms of E31 are all clustered within a 5 Å radius sphere in the apo structure of S100B($\beta\beta$), it is difficult to predict which of these residues is not a ligand in the Ca^{2+}-bound state.

The two regions of an S100β subunit with the least amount of sequence homology to other S100-family proteins are the hinge region and the C-terminal loop (loops II and IV respectively), and these loops are hypothesized to be responsible for the functional specificity of apo-S100B($\beta\beta$) and of S100 proteins in general (Kligman & Hilt, 1988). Interestingly, the hinge region and the C-terminal loop form a surface on the opposite side of the S100β subunit from the Ca^{2+}-binding loops as shown in Figures 5 and 7. The exposure of these loops is ideal for interactions with target proteins. In fact, a peptide from the hinge region of CP-10 (another S100 protein) was synthesized and found to exhibit chemotactic activity similar to the corresponding full-length protein, although sustained activity required the entire protein (Lackmann *et al.*, 1993). A role for the C-terminal loop in target molecule binding is supported by results from mutagenesis studies of another S100 protein, p11, where C82Q, Y85A, and F86A (corresponding to C84, F87, and F88 in S100β) mutations caused large decreases in annexin I binding (Kube *et al.*, 1992; Krebs *et al.*, 1995; Potts *et al.*, 1995). However, in apo-S100B($\beta\beta$), both F87 and F88 are clearly involved in intermolecular interactions with F14′ and F70′. Thus, as Krebs *et al.* suggested previously for calcyclin, the participation of these residues in the dimer interface raises new and important questions regarding the physiological significance of dimerization for S100 proteins (Krebs *et al.*, 1995; Potts *et al.*, 1995). The role of C84 in binding the τ protein to both S100β and S100α further supports the importance of the C-terminal loop (loop IV) in binding target proteins (Baudier *et al.*, 1988). Our studies indicate that only a small conformational change in the hinge region of S100β is required upon the addition of Ca^{2+} to expose C84 to solvent. Furthermore, C84 is at the top of a large cleft defined by helices III, III′, IV, and IV′ (Figure 8) which could accommodate the binding of the τ peptide upon the addition of Ca^{2+}. Thus, in a manner similar to CP-10, p11, and calcyclin, the hinge region (loop II) and the C-terminal loop (loop IV) of each subunit are most likely involved in the interaction of S100B($\beta\beta$) with target proteins to generate its specific biological response.

ACKNOWLEDGMENT

We are grateful to Dr. Mike Summers for NMR time, to Drs. Sanjiv Shah, Dana Hilt, Apostolos Gittis, Chitrananda Abeygunawardana, and Dana Zimmer for their very helpful discussions, to Paul Wilder for performing the PKC inhibition assays, and to Todd Tenenholz for assistance with graphics programs. This study also made use of The National Magnetic Resonance Facility at Madison (NMRFAM), which is supported by NIH Grant RR02301 from the Biomedical Research Technology Program, National Center for Research Resources. Equipment in the NMRFAM was purchased with funds from the University of Wisconsin, the NFS Biological Instrumentation Program (Grant DMB-8415048), the NIH Biomedical Research Technology Program (Grant RR02781), and the U.S. Department of Agriculture. This study also made use of the NMR facility at the University of Maryland at Baltimore (UMAB). A 600 MHz NMR spectrometer in the UMAB NMR facility was purchased with funds from the University of Maryland and the NIH shared instrumentation grant program (S10RR10441).

REFERENCES

Abeygunawardana, C., Weber, D. J., Gittis, A. G., Frick, D. N., Lin, J., Miller, A.-F., Bessman, M. J., & Mildvan, A. S. (1995) *Biochemistry 34*, 14997−15005.

Albert, K. A., Wilson, C.-S., Nairn, A. C., & Greengard, P. (1984) *Proc. Natl. Acad. Sci. U.S.A. 81*, 3622−3625.

Allore, R., O'Hanlon, D., Price, R., Neilson, K., Willard, H. F., Cox, D. R., Marks, A., & Dunn, R. J. (1988) *Science 239*, 1311−1313.

Amburgey, J. C., Abildgaard, F., Starich, M. R., Shah, S., Hilt, D. C., & Weber, D. J. (1995) *J. Biomol. NMR 6*, 171−179.

Baudier, J., & Cole, R. D. (1988a) *J. Biol. Chem. 263*, 5856−5883.

Baudier, J., & Cole, R. D. (1988b) *Biochemistry 27*, 2728−2736.

Baudier, J., Glasser, N., & Gérard, D. (1986) *J. Biol. Chem. 261*, 8192−8203.

Baudier, J., Mochly-Rosen, D., Newton, A., Lee, S.-H., Koshland, D. E., & Cole, R.D. (1987) *Biochemistry 26*, 2886−2893.

Baudier, J., Delphin, C., Grunwald, D., Khochbin, S., & Lawrence, J. J. (1992) *Proc. Natl. Acad. Sci. U.S.A. 89*, 11627−11631.

Bax, A., & Davis, D. (1985) *J. Magn. Reson. 65*, 355−360.

Bax, A., & Pochapsky, S. (1992) *J. Magn. Reson. 99*, 638−643.

Bax, A., Ikura, M., Kay, L. E., & Zhu, G. (1991) *J. Magn. Reson. 91*, 174−178.

Brünger, A. T. (1992) *X-PLOR Version 3.1, A system for x-ray crystallography and NMR*, Yale University, New Haven, CT.

Bruno, J., Horrocks, W. D., & Zauhar, R. J. (1992) *Biochemistry 31*, 7016−7026.

Chaudhuri, D., Horrocks, W. D., Amburgey, J. C., & Weber, D. J. (1996) *Biophys. J. 70*, A211.

Clore, G. M., Nilges, M., Sukumaran, D. K., Brünger, A. T., Karplus, M., & Gronenborn, A. M. (1986) *EMBO J. 5*, 2729−2735.

Clore, G. M., Gronenborn, A. M., Nilges, M., & Ryan, C. A. (1987) *Biochemistry 26*, 8012−8013.

Cronce, D. T., & Horrocks, W. D. (1992) *Biochemistry 31*, 7963−7969.

Delaglio, F., Grzesiek, S., Vuister, G. W., Zhu, G., Pfeifer, J., & Bax, A. (1995) *J. Biomol. NMR 6*, 277−293.

Donato, R. (1991) *Cell Calcium 12*, 713−726.

Drohat, A. C., Amburgey, J. C., & Weber, D. J. (1995) *Bull. UMAB 17th Annu. Grad. Res. Day*, 31.

Drohat, A. C., Amburgey, J. C., Abildgaard, F., Starich, M. R., & Weber, D. J. (1996) *Biophys. J. 70*, A59.

Edison, A. S., Abildgaard, F., Westler, W. M., Mooberry, E. S., & Markley, J. L. (1994) *Methods Enzymol. 239*, 3−79.

Ferrin, T. E., Huang, C. C., Jarvis, L. E., & Langridge, R. (1988) *J. Mol. Graphics 6*, 13−27.

Folkers, P. J. M., Folmer, R. H. A., Kinings, R. N. H., & Hilbers, C. W. (1993) *J. Am. Chem. Soc. 115*, 3798−3799.
Gardner, J. (1995) *SeqVu, version 1.0*, Garvin Institute of Medical Research, Sydney, Australia.
Harris, N. L., Presnell, S. R., & Cohen, F. C. (1994) *J. Mol. Biol. 236*, 1356−1368.
Hilt, D. C., & Kligman, D. (1991) in *Novel Calcium-Binding Proteins* (Heizmann, C., Ed.) Springer, Berlin, FRG.
Horrocks, W. D., & Sudnick, D. R. (1981) *Acc. Chem. Res. 14*, 384−392.
Ikura, M., Bax, A., Clore, G. M., & Gronenborn, A. M. (1990) *J. Am. Chem. Soc. 112*, 9020−9022.
Jeener, J., Meier, B. H., Bachmann, P., & Ernst, R. R. (1979) *J. Chem. Phys. 71*, 4546−4553.
Kay, L. E., & Bax, A. (1990) *J. Magn. Reson. 86*, 110−126.
Kay, L. E., Marion, D., & Bax, A. (1989) *J. Magn. Reson. 84*, 72−84.
Kessler, H., Griesinger, C., Kerssebaum, R., Wagner, K., & Ernst, R. R. (1987) *J. Am. Chem. Soc. 109*, 607−609.
Kligman, D., & Marshak, D. R. (1985) *Proc. Natl. Acad. Sci. U.S.A. 82*, 7136−7139.
Kligman, D., & Hilt, D. C. (1988) *Trends Biochem. Sci. 13*, 437−443.
Krebs, J., Quadroni, M., & Van Eldik, L. J. (1995) *Nat. Struct. Biol. 2*, 711−714.
Kretsinger, R. H. (1980) *CRC Crit. Rev. Biochem. 8*, 119−174.
Kube, E., Becker, T., Weber, K., & Gerke, V. (1992) *J. Biol. Chem. 267*, 14175−14182.
Kuboniwa, H., Tjandra, N., Grzesiek, S., Ren, H., Klee, C. B., & Bax, A. (1995) *Nat. Struct. Biol. 2*, 768−776.
Lackmann, M., Rajasekariah, P., Iismaa, S. E., Jones, G., Cornish, C. J., Hu, S., Simpson, R. J., Moritz, R. L., & Geczy, C. L. (1993) *J. Immunol. 150*, 2981−2991.
Laskowski, R. A., McArthur, M. W., Moss, D. S., & Thornton, J. M. (1993) *J. Appl. Crystallogr. 26*, 283−291.
Lin, L.-H., Van Eldik, L. J., Osheroff, N., & Norden, J. J. (1994) *Mol. Brain Res. 25*, 297−304.
Live, D. H., Davis, D. G., Agosta, W. C., & Cowburn, D. (1984) *J. Am. Chem. Soc. 106*, 1939−1941.
Marion, D., Ikura, M., Tschudin, R., & Bax, A. (1989) *J. Magn. Reson. 85*, 393−399.
McCoy, M. A., & Mueller, L. (1992) *J. Am. Chem. Soc. 114*, 2108−2112.
Moore, B. E. (1965) *Biochem. Biophys. Res. Commun. 19*, 739−744.
Muhandiram, D. R., Farrow, N. A., Xu, G.-Y., Smallcombe, S. H., & Kay, L. E. (1993a) *J. Magn. Reson. B102*, 317−321.
Muhandiram, D. R., Guang, Y. X., & Kay, L. E. (1993b) *J. Biomol. NMR 3*, 463−470.
Nilges, M. (1993) *Proteins: Struct., Funct., Genet. 17*, 297−309.
Palmer, A. G., Cavanaugh, J., Wright, P. E., & Rance, M. (1991) *J. Magn. Reson. 93*, 151−170.
Patel, J., & Kligman, D. (1987) *J. Biol. Chem. 262*, 16686−16691.
Patel, J., Marangos, P. J., Heydorn, W. E., Chang, B., Verma, A., & Jacobowitz, D. (1983) *J. Neurochem. 41*, 1040−1046.
Potts, B. C. M., Smith, J., Akke, M., Macke, T. J., Okazaki, K., Hidaka, H., Case, D. A., & Chazin, W. J. (1995) *Nat. Struct. Biol. 2*, 790−796.
Reeves, R. H., Yao, J., Crowley, M. R., Buck, S., Zhang, X., Yarowsky, P., Gearhart, J. D., & Hilt, D. C. (1994) *Proc. Natl. Acad. Sci. U.S.A. 91*, 5359−5363.
Sack, J. S. (1988) *J. Mol. Graphics 6*, 244−245.
Schäfer, B. W., Heizmann, C. W. (1996) *Trends Biochem. Sci. 21*, 134−140.
Shaka, A. J., Keler, J., & Freeman, R. (1983) *J. Magn. Reson. 53*, 313−340.
Shaka, A. J., Barker, P., & Freeman, R. (1985) *J. Magn. Reson. 64*, 547−552.
Sheu, F.-S., Azmitia, E. C., Marshak, D. R., Parker, P. J., & Routtenberg, A. (1994) *Mol. Brain Res. 21*, 62−66.
Shinnar, M., Bolinger, L., & Leigh, J. S. (1989a) *Magn. Reson. Med. 12*, 88−92.
Shinnar, M., Eleff, S., Subramanian, H., & Leigh, J. S. (1989b) *Magn. Reson. Med. 12*, 74−80.
Skelton, N. J., Forsén, S., & Chazin, W. J. (1990) *Biochemistry 29*, 5752−5761.
Spera, S., & Bax, A. (1991) *J. Am. Chem. Soc. 113*, 5490−5492.
Starich, M. (1995) *Diss. Abstr.* (in press).
Strynadka, N. C. J., & James, M. N. G. (1989) *Annu. Rev. Biochem. 58*, 951−998.
Szebenyi, D. M. E., & Moffat, K. (1986) *J. Biol. Chem. 261*, 8761−8777.
Van Eldik, L. J., & Griffin, W. S. T. (1994) *Biochim. Biophys. Acta 1223*, 398−403.
Vuister, G. W., & Bax, A. (1992) *J. Magn. Reson. 98*, 428−435.
Vuister, G. W., Clore, G. M., Gronenborn, A. M., Powers, R., Garrett, D. S., Tschudin, R., & Bax, A. (1993) *J. Magn. Reson. B101*, 210−213.
Wilder, P. T., & Weber, D. J. (1996) *Biophys. J. 70*, A62.
Wüthrich, K. (1986) *NMR of Proteins and Nucleic Acids*, John Wiley, New York.
Zimmer, D. B., Cornwall, E. H., Landar, A., & Song, W. (1995) *Brain Res. Bull. 37*, 417−429.
Zhu, G., & Bax, A. (1990) *J. Magn. Reson. 90*, 405−410.
Zhu, G., & Bax, A. (1992) *J. Magn. Reson. 98*, 192−199.

BI9612226